Clay Minerals, (2016) **51**, 747–762

Vermiculite expansion through non-artificial processes in pyroclastic carbonatites from Catanda (Angola)

J. XU[1,*], M. CAMPENY[1], E. TAULER[1], J.C. MELGAREJO[1] AND A.O. GONÇALVES[2]

[1] *Departament de Mineralogia, Petrologia i Geologia Aplicada, Facultat de Geologia, Universitat de Barcelona, C/Martí i Franquès s/n, 08028 Barcelona, Spain*
[2] *Departamento de Geologia, Universidade Agostinho Neto, Luanda, Angola*

(*Received 25 March 2016; revised 29 July 2016; Associate Editor: Juan Cornejo*)

ABSTRACT: The pyroclastic carbonatitic rocks from the Catanda volcanic area (Angola) contain annite and phlogopite grains which have been affected to a significant extent by vermiculitization. A mineralogical study of these micas has revealed that the annite was altered to K-vermiculite while vermiculitization of phlogopite generated Ca-vermiculite. Intermediate alteration products such as intergrowths of phlogopite/Ca-vermiculite were also found, but interstratified crystals of phlogopite/vermiculite, a common intermediate product during vermiculitization processes, are not reported in the Catanda rocks. The two types of vermiculitized micas show 'accordion' textures, related to the expansion of vermiculite. To the authors' knowledge, the present study is the first report of expanded vermiculites described in natural rocks and not generated as a consequence of industrial processing.

KEYWORDS: vermiculite expansion, annite, phlogopite, carbonatite, Catanda, Angola.

Vermiculite is a 2:1 clay mineral. It may be either dioctahedral or trioctahedral and contains interlayer cations and two sheets of water molecules, presenting a layer charge of 0.6–0.9 e/huc (Bailey, 1980; Guggenheim *et al*., 2006). Vermiculite is normally formed by the alteration of primary micas such as annite $[KFe^{2+}_3AlSi_3O_{10}(OH)_2]$ or phlogopite $[KMg_3AlSi_3O_{10}(OH)_2]$, in a process known as vermiculitization (Deer *et al*., 1962), and this has been reported extensively from various lithologies and locations worldwide (Moon *et al*., 1994; Toksoy-Köksal *et al*., 2001; Azzone & Ruberti, 2010).

Commercially, the term vermiculite is used to describe micaceous minerals that can be exfoliated and expanded under rapid heating. When submitted to a rapid increase in temperature vermiculite loses its interlayer water which is converted to vapour. This process generates significant internal pressure leading to the exfoliation of the vermiculite crystals and a general expansion of the grain (Huo *et al*., 2012; Hillier *et al*., 2013). Expanded vermiculites increase to up to 30 times their original volume, generating typical 'accordion' or 'concertina-like' textures (Walker, 1951; Hindman, 2006; Hillier *et al*., 2013). This peculiar property of vermiculite has triggered a widespread commercial interest in this mineral as a substrate in hydroponics or as an absorber of moisture or contaminants, among other applications (Huo *et al*., 2012). The expansion of vermiculite is commonly produced by artificial heating up to ~900°C for a few minutes in a furnace, using hydrogen peroxide (H_2O_2) or microwaves (Hindman, 2006; Marcos *et al*., 2009; Marcos & Rodríguez, 2010; Huo *et al*., 2012; Hillier *et al*., 2013). In addition, several studies have indicated

* E-mail: jingyao.xu@ub.edu
https://doi.org/10.1180/claymin.2016.051.5.05

that rapid heating up to 300°C can also produce vermiculite expansion (Deer *et al*., 1966; Hillier *et al*., 2013).

Vermiculite accordion textures generated by thermal expansion have not been reported other than as a result of artificial processes. The lack of natural examples of expanded vermiculites is probably due to the fact that vermiculitization is a low-temperature process in which the suitable conditions of heating are not likely to produce its expansion.

However, during the present petrographic study carried out on the carbonatitic pyroclastic rocks of Catanda (Angola), mineral phases corresponding to the biotite series (Rieder *et al*., 1998, 1999) affected by vermiculitization were identified. These grains also present accordion textures similar to those reported in vermiculite grains submitted to artificial heating (Marcos *et al*., 2009; Hillier *et al*., 2013).

In the present study the alteration patterns of the Catanda micas during vermiculitization are established and the processes related to the formation of the Catanda accordion textures are characterized.

GEOLOGICAL SETTING

Carbonatites are magmatic rocks – plutonic, volcanic or hypabyssal – containing >50% modal carbonates. They are typified geochemically by large abundances of Sr, Ba or P (Nelson *et al*., 1988) and by significant enrichment in 'Hi-tech' metals (*e.g.* rare earth elements (*REE*), Nb, Ta), which has generated much interest in these rocks over recent years (*e.g.* Wyllie *et al*., 1996; Chakhmouradian, 2006). To date, 520 carbonatites have been reported worldwide, 50 of which are related to volcanism, but carbonatitic lavas have only been reported in 14 localities (Woolley & Church, 2005). One of these localities is the Catanda volcanic area (Silva & Pereira, 1973) located in the Kwanza Sul province, ~350 km SE of Luanda (Angola) (Fig. 1). Recent studies reveal that Catanda carbonatites are formed by small monogenetic volcanic cones made up of a series of pyroclastic rocks with minor interbedded carbonatitic lavas (Campeny *et al*., 2014).

The pyroclastic rocks of the Catanda area consist of carbonatitic minerals (calcite, fluorapatite, titaniferous magnetite, pyrochlore, baddeleyite and phlogopite)

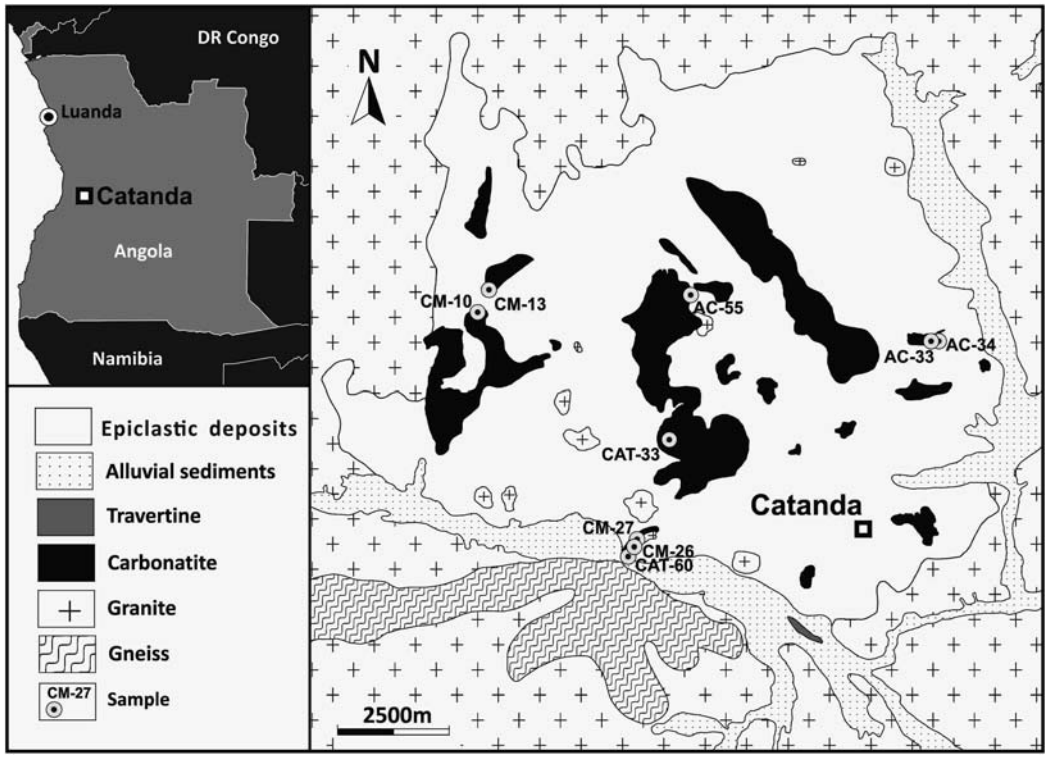

FIG. 1. Location and geological setting of the Catanda carbonatitic volcanic area (modified from Campeny *et al*., 2014).

https://doi.org/10.1180/claymin.2016.051.5.05 Published online by Cambridge University Press

and xenocrysts, from the host Archaean granites, of quartz, microcline, plagioclase and annite. Secondary minerals such as vermiculite and rhabdophane are also present (Campeny *et al*., 2014).

METHODS

The present study was based on the analysis of 26 samples of pyroclastic carbonatites collected in the Catanda area. Petrographic and textural studies of the samples were carried out using optical and scanning electron microscopy (SEM), the latter employing an E-SEM-Quanta 200 FEI-XTE-325/D8395.BSE instrument coupled to a Genesis EDS microanalysis system at the Scientific and Technical Centres of the University of Barcelona (CCiTUB). The operating conditions were 20 kV, 1 nA beam current and 10 mm distance to detector.

The mineralogical compositions of the samples were determined by X-ray diffraction (XRD) using a PANalytical X'Pert PRO-MPD-Alpha1 powder diffractometer with a θ/2θ Bragg-Brentano geometry and 240 mm radius. Instrumental and experimental conditions were 45 kV, 40 mA with Cu-$K\alpha_1$ radiation (λ = 1.5406 Å), primary Ge monochromator (111), sample rotation at 2 revolutions s^{-1}, automatic variable divergence slit to obtain an illuminated length of 10 mm, and an X'Celerator detector with an active length of 2.122°. Analyses were carried out in the θ/2θ range of 4–80°, using a step size of 0.017°, and a measuring time of 50 s per step. Powedered samples were prepared and the results were treated using *X'Pert HighScore Plus* v.2.2.2 software and *Powder Diffraction File (version 2)* (Joint Committee of Powder Diffraction Standards, 2000). The XRD profile adjustment was carried out using *TOPAS* (2009) software in order to obtain the semi-quantitative percentage and the cell parameters of the mineral phases. The phyllosilicate structures used in *TOPAS* (2009) were obtained from Shirozu & Bailey (1966), Brigatti *et al*. (2000) and Schingaro *et al*. (2001). Oriented mounts were used to identify clay minerals. Samples were analysed using XRD at room temperature and pressure, treated with ethylene glycol and heated to 550°C (Thorez, 1975).

A compositional study of the phyllosilicates was carried out using an electron microprobe (EMPA) (JEOL JXA-8230), equipped with five wavelength dispersive spectrometers (WDS) and an energy dispersive spectrometer (EDS). The operating conditions were: accelerating voltage of 20 kV combined with a beam current of 6.9 nA for Na and F; 14 nA for Al, Ti, K and Sr; 15 nA for Mn, Ba and Ca; 16 nA for Si, Mg and Cr, and 19 nA for Fe. Calibration standards and analytical crystals used for the analyses were: corundum (Al, TAP, Kα), wollastonite (Si, TAP, Kα), rutile (Ti, PETJ, Kα), periclase (Mg, TAPH, Kα), albite (Na, TAPH, Kα), fluorite (F, TAPH, Kα), Fe_2O_3 (Fe, LIFH, Kα), rhodonite (Mn, LIFH, Kα), baryte (Ba, LIFH, Lα), chromite (Cr, PETL, Kα) wollastonite (Ca, PETL, Kα), orthoclase (K, PETL, Kα) and celestite (Sr, PETL, Lα). The structural formulae of micas were calculated based on 12(O, OH, F). All iron present was assumed to be Fe^{2+} in micas and Fe^{3+} in vermiculite and the intermediate grains of mica-vermiculite.

RESULTS

Petrography

Pyroclastic Catanda rocks consist of carbonatitic juveniles (pyroclastic fragments derived directly from magma) 3 mm in diameter consisting of calcite, fluorapatite, titaniferous magnetite, pyrochlore, baddeleyite and phlogopite (Fig. 2a). Xenocrysts and rock fragments up to 5 mm across (mainly of quartz, microcline, plagioclase and annite) which originated in the host Archaean granites were also noted. Glimmeritic xenoliths, composed mainly of phlogopite, were also reported forming grains up to 2 mm across (Campeny *et al*., 2014).

Phyllosilicates

Catanda phyllosilicates consist of tabular crystals of phlogopite and annite up to 3 mm long, distinguished by their pleochroism – yellow to brownish in phlogopite and brownish to dark brown in annite. In addition, thicker grains defining accordion textures are also present, with interstitial micritic or sparitic calcite (Fig. 2b). According to these textures, the Catanda phyllosilicates are classified here as: (a) non-expanded phlogopite and annite (Fig. 3a1, a2); (b) slightly expanded phyllosilicate grains with interstitial sparitic calcite (Fig. 3b1,b2); (c) strongly expanded phyllosilicate crystals, defining accordion textures and presenting interstitial sparitic calcite (Fig. 3c1,c2); and (d) phyllosilicate accordions partially or completely replaced by calcite (Fig. 3d1,d2).

Significant alteration processes related to the formation of vermiculite have affected the Catanda phyllosilicates. This vermiculite can be distinguished easily using SEM-EDS in back-scattered electron (BSE) mode, as low-density areas (dark grey), while lighter regions correspond to primary phlogopite or annite (Fig. 4).

https://doi.org/10.1180/claymin.2016.051.5.05 Published online by Cambridge University Press

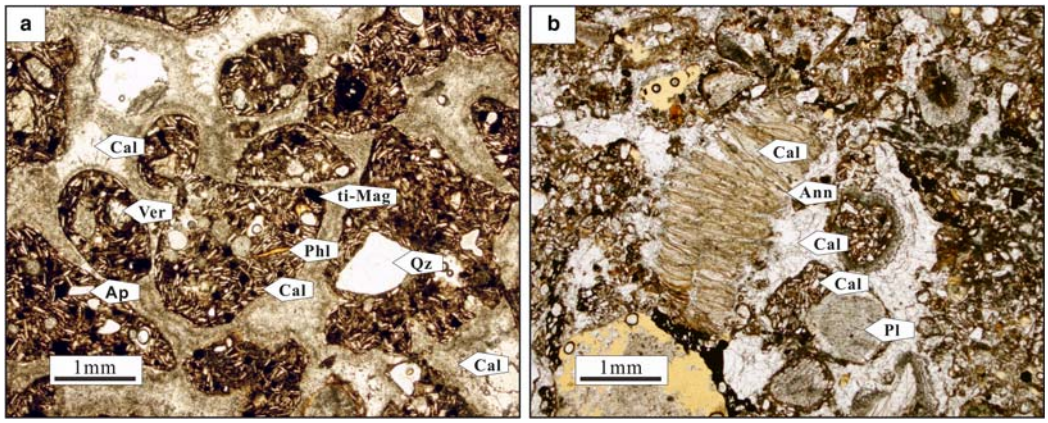

FIG. 2. Plane-polarized light photomicrographs. (a) View of a carbonatitic pyroclastic rock from Catanda (sample CM-10) with 'juveniles' (pyroclastic fragments derived directly from magma) consisting of tabular calcite (Cal), titaniferous magnetite (ti-Mag), phlogopite (Phl), vermiculite (Ver), fluorapatite (Ap) and fragments from the Archaean granites such as quartz (Qz). (b) Vermiculitized and expanded annite (Ann) grain defining a typical accordion texture, from sample CM-26. Juvenile fragments consist mainly of tabular magmatic calcite (Cal, type1) and minor xenocrysts such as plagioclase (Pl), and are cemented by diagenetic sparitic calcite (Cal, type2).

XRD characterization of the phyllosilicates

The Catanda phyllosilicates were also studied using oriented preparations, in order to confirm the observations made during petrographic and textural studies in which primary phyllosilicates (annite and phlogopite) and secondary vermiculite were identified. The Catanda vermiculite has a d_{002} spacing of 14.5–14.8 Å, measured at room conditions and after treatment with ethylene glycol. This diffraction maximum of vermiculite collapses to 10 Å after heating at 550°C, which is similar to the d_{001} value of micas (Fig. 5). The d_{001} spacing in micas is 10 Å, and it is not affected by ethylene glycol treatment or by heating at 550°C. In the samples studied no interstratified mica/vermiculite, which generally has a d_{002} diffraction maximum at 12 Å, was identified.

Furthermore, phyllosilicate contents were calculated from random mounts using the *TOPAS* (2009) software. Due to the large percentage of calcite (69–87 wt.%) the intensity of the diffraction peaks of the other minerals was very low (Fig. 6a). A carbonate-free fraction was obtained by dilute-acid attack to improve the XRD trace and the Rietveld study on this fraction was then repeated. The calcite content was determined by means of the 'Bernard calcimeter' (Hülsemann, 1966) (sample CAT-33 contains 72 wt.% calcite). The semi-quantitative results of carbonate-free fractions are listed in Table 1. The XRD profiles before and after removal of the carbonates are shown (Fig. 6).

For XRD profile adjustment it was assumed that annite has a 1*M* polytype structure belonging to the *C*2/*M* space group, cell parameters of $a = 5.336$ Å, $b = 9.239$ Å, $c = 10.200$ Å, $\beta = 100.29°$ and a cell volume $= 494.77$ Å^3 (Brigatti *et al*., 2000). Phlogopite has a 1*M* polytype structure belonging to the *C*/2*M* space group, with cell parameters of $a = 5.327$ Å, $b = 9.225$ Å, $c = 10.236$ Å, $\beta = 99.99°$ and a cell volume of 495.39 Å^3 (Schingaro *et al*., 2001). Vermiculite belongs to the *Cc* space group with cell parameters of $a = 5.349$ Å, $b = 9.255$ Å, $c = 28.840$ Å, $\beta = 97.12°$ and a cell volume of 1419.17 Å^3 (Shirozu & Bailey, 1966). In the profile adjustment, the composition of phyllosilicates analysed by EMPA was introduced. Table 2 lists the cell parameters calculated using *TOPAS* for annite, phlogopite and vermiculite before and after acid treatment. The interlayer space of the vermiculite would have been affected by the acid treatment, but not that of the micas. There are no significant differences between the cell parameters and the cell volume of annite and phlogopite compared with the values obtained by Schingaro *et al*. (2001) and Brigatti *et al*. (2000). In the sample without acid treatment, CAT-33, the d_{002} of vermiculite is 14.5 Å; in samples CAT-60 and AC-55 it is 14.7 Å, and in CM-10 it is 14.8 Å. The cell volume of the Catanda vermiculite is larger than that reported by Shirozu & Bailey (1966), which may be due to the compositional variations in the interlayer position.

https://doi.org/10.1180/claymin.2016.051.5.05 Published online by Cambridge University Press

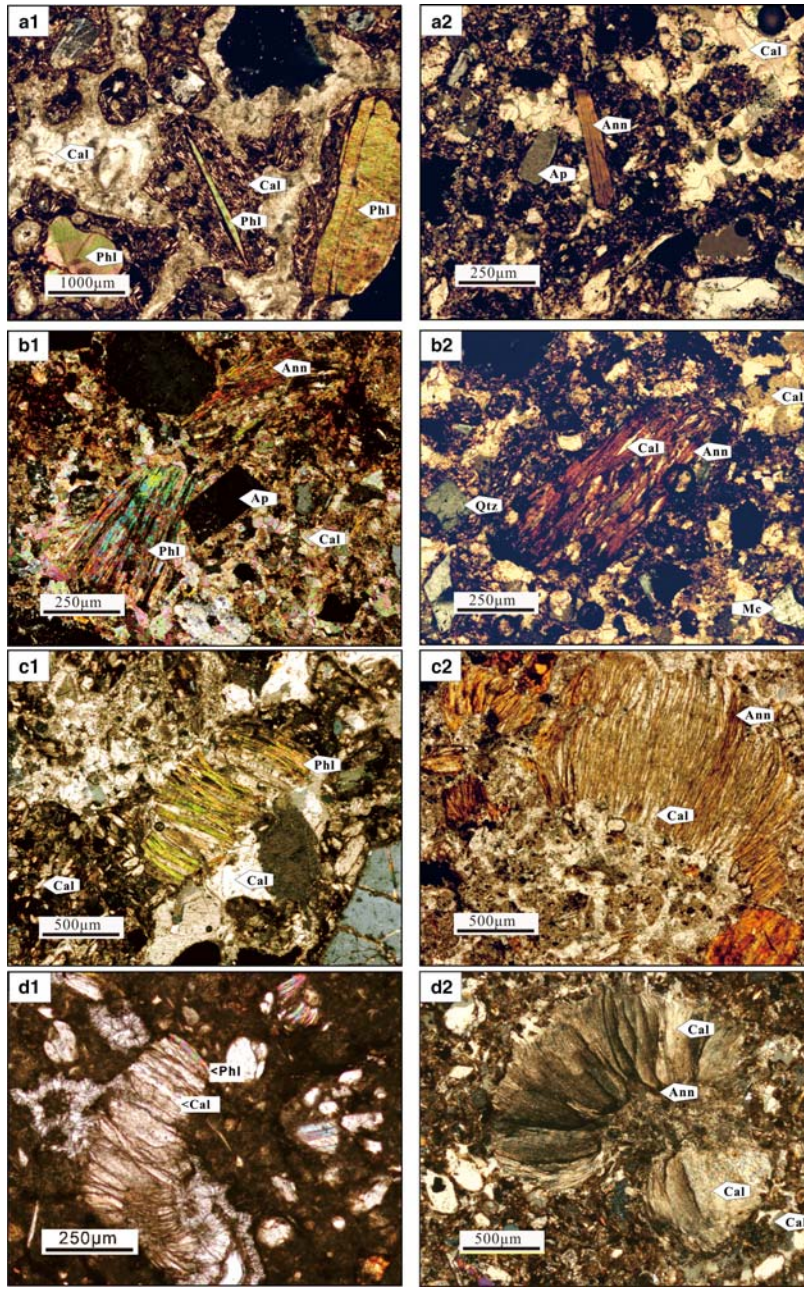

FIG. 3. Plane-polarized light photomicrographs. (a1) General view of a Catanda pyroclastic rock sample (CM-10) with an un-expanded tabular grain of phlogopite (Phl) accompanied by apatite (Ap) and sparitic calcite as cement; (a2) tabular fresh crystal of annite (Ann) acting as the core of a juvenile fragment, from sample AC-55; (b1) expanded grains of annite (Ann) and phlogopite (Phl), sample CM-26; (b2) expanded crystal of annite (Ann) with interlayer sparitic calcite, sample AC-55; (c1) significantly expanded phlogopite (Phl) defining a typical accordion texture with sparitic calcite in the cleavage surfaces, sample CM-26; (c2) expanded annite grain with accordion texture and calcite filling, sample CM-13; (d1) expanded phlogopite-vermiculite replaced by micritic calcite (Cal), sample CM-27; (d2) annite-vermiculite accordion replaced completely by micritic calcite, sample CAT-30.

https://doi.org/10.1180/claymin.2016.051.5.05 Published online by Cambridge University Press

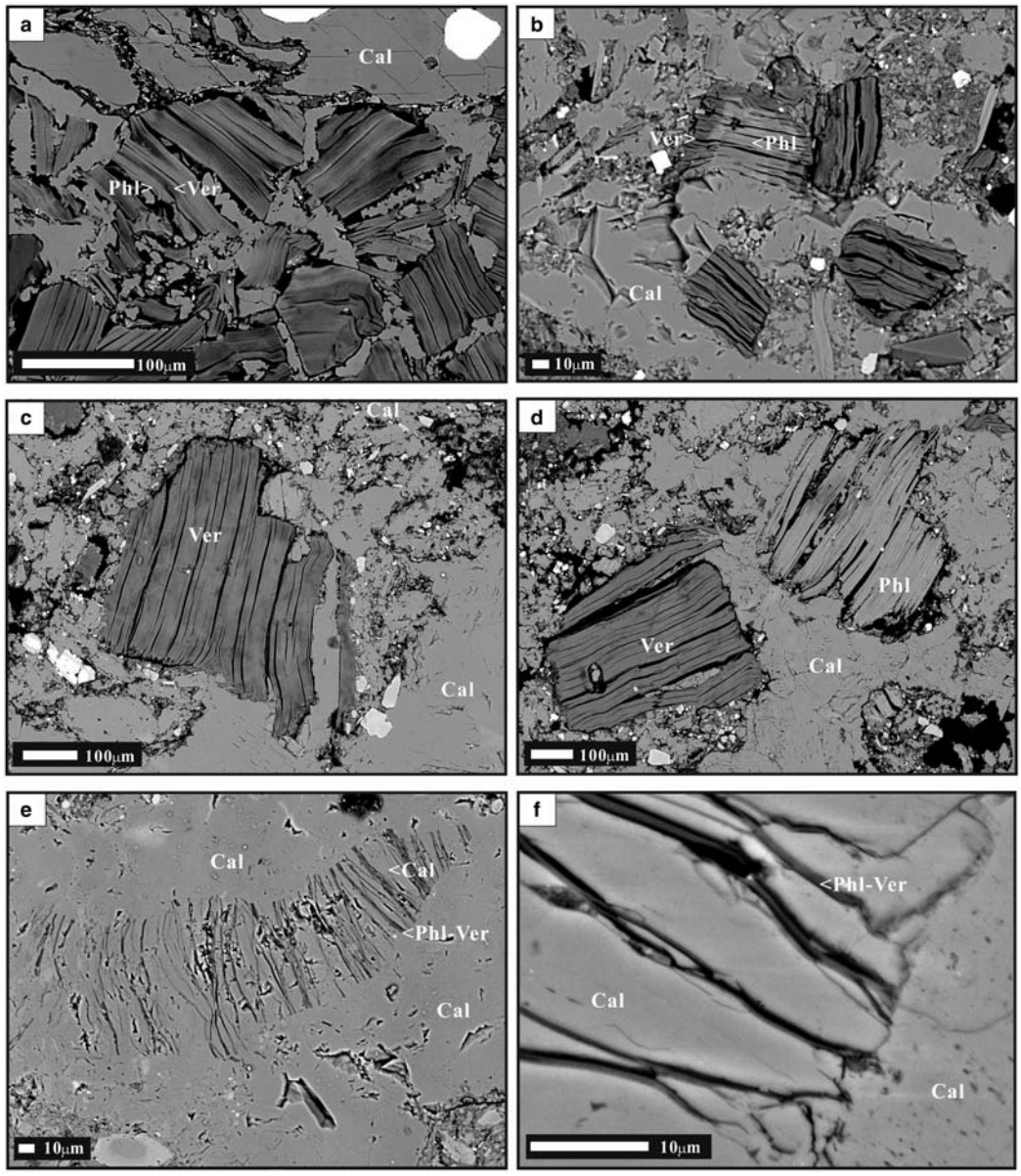

FIG. 4. SEM (BSE) images of the phyllosilicates from the Catanda pyroclastic rocks. (a) Phlogopite (Phl) grain partially altered to vermiculite (Ver) along its exfoliation planes, from sample AC-55; (b) Phlogopite (Phl) crystal partially altered to vermiculite (Ver); the vermiculitization is progressing from the rim to crystal core, sample CAT-60; (c) inhomogeneous vermiculite grain; the darker patches contain less K than the lighter area, from sample AC-34; (d) individual grains of phlogopite (Phl) and vermiculite which can be distinguished by the different contrast, sample AC-34; (e) expanded grain of phlogopite-vermiculite (Phl-Ver) with typical accordion texture; sparitic calcite (Cal) fills the interlayer space generated during the thermal expansion, sample CM-27; (f) enlarged view of a phlogopite-vermiculite accordion, sample CAT-33.

https://doi.org/10.1180/claymin.2016.051.5.05 Published online by Cambridge University Press

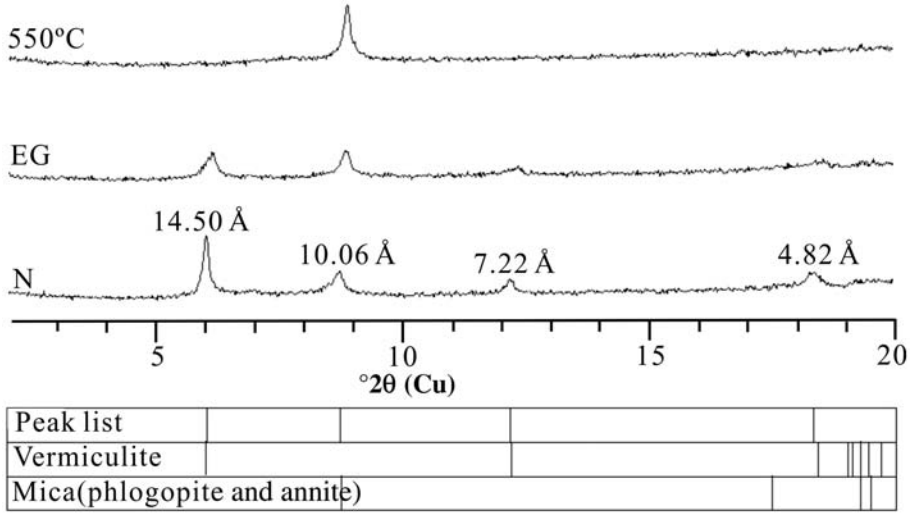

FIG. 5. XRD patterns, obtained by the oriented-aggregate method, of sample CAT-33, before acid treatment. Vermiculite shows a maximum at 14.5 Å, collapses at 10 Å and does not expand with ethylene glycol. The lower part of the figure shows the peak list and the Bragg position of each mineral. N: room temperature; H550: heated to 550°C; EG: ethylene glycol.

Mineral chemistry

The alteration of micas to vermiculite is a continuous process, acting at all scales, probably beyond the resolution of BSE imaging, at the lattice scale, as described for other cases of intergrown phyllosilicate grains (*e.g.* Giorgetti *et al*., 1997). Hence, compositional boundaries cannot be established clearly in the altered grains. In the present study, micas were considered as pure phases when the K_2O content was >7 wt.% and the interlayer charge was 0.85–1.0 e/f.u. (electron per formula unit) (Guggenheim *et al*., 2006). Classification within the phlogopite–annite series was carried out according to the ratio #Mg = Mg/(Mg + Fe), considering that phlogopite has #Mg > 0.5 and annite #Mg < 0.5 (Tischendorf *et al*., 2007). Whereas Hillier *et al*. (2013) considers pure vermiculite to contain <1 wt.% K_2O , according to Azzone & Ruberti (2010), pure vermiculite has < 0.125 a.p.f.u. (atoms per formula unit) of K . In Catanda, the phyllosilicates analysed have an interlayer charge of 0.6–0.85 e/f.u. and so cannot be considered as pure micas. Nevertheless, they do represent intermediate components between mica and vermiculite or even pure K-vermiculite. In the present study, pure vermiculite (Ca- or Mg-vermiculite, not K-vermiculite) was considered to have a K content of < 0.125 a.p.f.u.; K contents of > 0.125 a.p.f.u. correspond to intermediate components of mica-vermiculite or K-vermiculite.

Representative EMPA analyses of pure micas (annite and phlogopite) from Catanda are shown in Table 3. In the intermediate mica-vermiculite grains, Al ranges from 0.81 to 1.29 a.p.f.u. in the tetrahedral sheet and from 0 to 0.27 a.p.f.u. in the octahedral sheet. The sum of the octahedral cations is 2.46–3.00 a.p.f.u., while the interlayer position is occupied by K (0.01–0.76 a.f.u), Ca (0–0.32 a.p.f.u.), Na (0.01–0.21 a.p.f.u.), Mg (0–0.06 a.p.f.u.) and Sr (0–0.01 a.p.f.u.). Representative compositional relationships of intermediate mica-vermiculite crystals are shown in Fig. 7.

Pure vermiculite (Ca-vermiculite) has tetrahedral sites occupied by Si (2.99–3.20 a.p.f.u.), Al (0.81–1.02 a.p.f.u.) and Fe^{3+} (0–0.03 a.p.f.u.), while the octahedral position is mainly occupied by Mg (2.26–2.68 a.p.f.u.), Fe^{3+} (0.529–0.50 a.p.f.u.), Al (0–0.1 a.p.f.u.), Ti (0.01–0.04 a.p.f.u.), Mn (0.01–0.04 a.p.f.u.) and Cr (0–0.01 a.p.f.u.). All pure vermiculites (Ca-vermiculite) have a Mg/(Fe + Mg) ratio of >0.82. Catanda vermiculite presents Ca (0.22–0.32 a.p.f.u.) as the main interlayer cation, though other minor elements such as Mg (0–0.06 a.p.f.u.), Na (0.01–0.21 a.p.f.u.) and K (0.01–0.01 a.p.f.u.) are also present. Considering the composition of the interlayer cation, Catanda vermiculite should be considered a Ca-vermiculite. A few representative compositional EMPA analyses, and the structural formulae of pure vermiculite from Catanda, are summarized in Table 4.

https://doi.org/10.1180/claymin.2016.051.5.05 Published online by Cambridge University Press

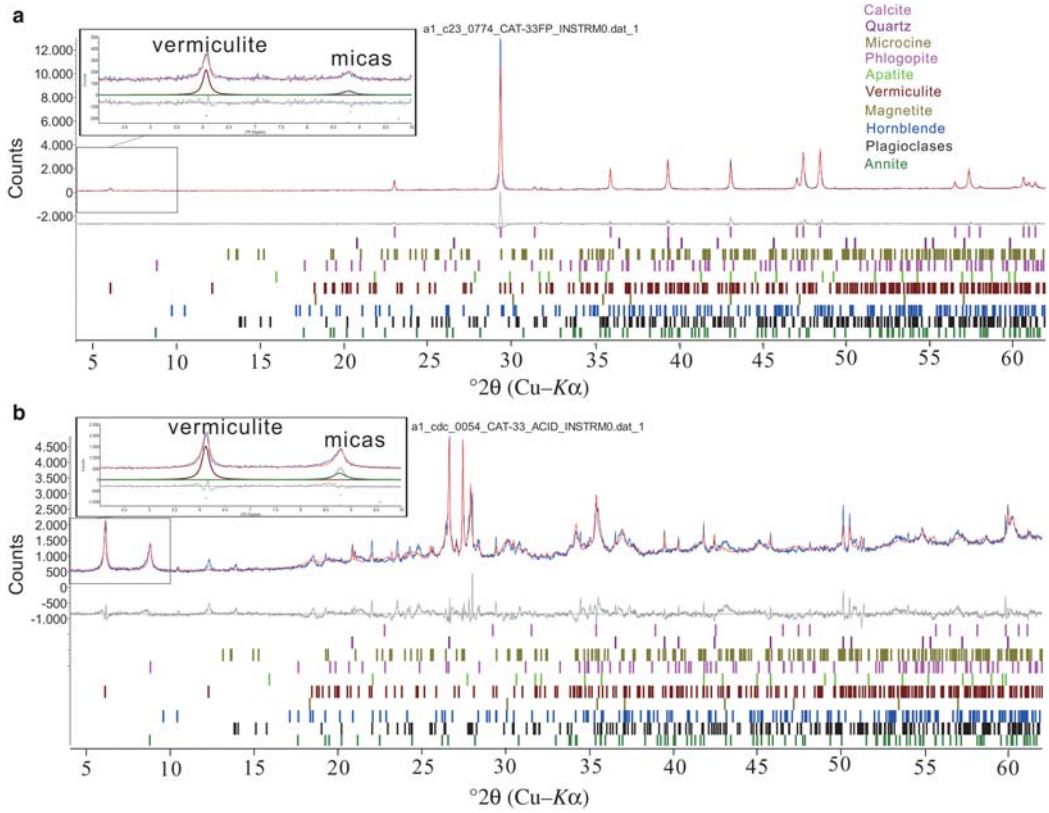

FIG. 6. XRD profiles and semi-quantitative analyses of sample CAT-33 using the powder method and the *TOPAS* (2009) software. (a) Sample before acid treatment; (b) sample after acid treatment. In the left top corner of both parts, a diffraction peaks area corresponding to d_{002} of vermiculite and d_{001} of micas and the calculated profile of the phyllosilicates are shown. The calculated profile is shown in red, the experimental profile is shown in blue and the difference between the two is shown in grey.

Compositional diagrams comparing the relationship between the interlayer cation/Si *vs*. Al/Si and $(Fe + Mg)^{VI}$/Si (Fig. 7a,b) do not show a clear tendency when comparing Catanda vermiculites and micas, due to the wide range of compositions of the original phlogopites. Pure micas from Catanda are mostly enriched in Mg and plot mainly in the field of phlogopite, though a few analyses fit within the annite compositions (Fig. 7c). All of the analyses carried out on pure Ca-vermiculite, *i.e.* those presenting $K < 0.125$, have octahedral $\#Mg > 0.5$. The relationship between K and $Ca + Mg + Na$ in the vermiculite interlayer space shows that the decrease in K was compensated by the addition of Ca, Mg and Na during the vermiculitization process (Fig. 7d; Table 5).

This compositional study of the phyllosilicates suggests that intermediate mica-vermiculite grains are sometimes expanded forming accordion textures; these are not present in pure vermiculite grains.

DISCUSSION

Vermiculitization of phlogopite

Previous work (Moon *et al*., 1994; Azzone & Ruberti, 2010) has proposed that vermiculitization of micas proceeds as follows: mica → interstratified mica-vermiculite → vermiculite, and this is determined by XRD which is used to identify peaks at 10, 12 and 14 Å, respectively. In the present study of the Catanda samples peaks at 10 and 14 Å only, were identified,

https://doi.org/10.1180/claymin.2016.051.5.05 Published online by Cambridge University Press

TABLE 1. Semi-quantitative proportions of minerals from the Catanda pyroclastic rocks after acid treatment (carbonate-free fraction), calculated using the *TOPAS* (2009) software.

Sample	Quartz	Microcline	Plagioclase	Apatite	Magnetite	Vermiculite	Mica (phlogopite/annite undifferentiated)	Hornblende	Calcite (residual)
AC-55	1	33	19	6	16	1	23	0	1
CAT-33	5	11	12	4	19	8	40	0	0
CAT-60	15	13	14	2	12	5	37	0	1
CM-10	3	9	25	12	23	12	10	5	2

while the peak at 12 Å, corresponding to the intermediate stage of interstratified mica-vermiculite, was not detected. It is concluded, therefore, that the Catanda intermediate product of phlogopite-vermiculite should not be considered as an interstratified phlogopite-vermiculite. Hence, the altered Catanda

TABLE 2. Rietveld-refined cell parameters of annite, phlogopite and vermiculite from Catanda after acid treatment and of vermiculite before acid treatment.

Sample		After acid treatment			Before acid treatment
		Annite	Phlogopite	Vermiculite	Vermiculite
AC-55	*a* (Å)	5.3237(33)	5.2342(17)	5.589(54)	5.572(72)
	b (Å)	9.2050(53)	9.0000(33)	8.900(80)	8.97(11)
	c (Å)	10.1913(26)	10.199(17)	29.37(13)	29.92(18)
	β (°)	99.703(34)	99.632(99)	98.92(96)	99.2(13)
	Cell volume (Å)^3	492.28(44)	473.67(83)	1443(20)	1477(28)
			Rwp = 10.61		*Rwp* = 12.84
CAT-33	*a* (Å)	5.3189(20)	5.2213(26)	5.5900(38)	5.590(11)
	b (Å)	9.2204(33)	9.0181(42)	8.9377(60)	9.000(16)
	c (Å)	10.1965(34)	10.1591(29)	29.156(13)	29.480(32)
	β (°)	99.321(31)	98.842(34)	98.318(76)	98.94(21)
	Cell vol. (Å)^3	493.46(31)	472.67(35)	1441.4(15)	1465.1(43)
			Rwp = 7.14		*Rwp* = 10.76
CAT-60	*a* (Å)	5.3244(21)	5.2246(31)	5.5857(70)	5.5791(54)
	b (Å)	9.1973(35)	9.0015(57)	8.903(10)	8.9724(79)
	c (Å)	10.2028(31)	10.224(10)	29.097(21)	29.880(17)
	β (°)	99.563(29)	99.280(85)	98.31(13)	98.85(10)
	Cell vol. (Å)^3	492.69(31)	474.56(63)	1431.8(27)	1477.9(21)
			Rwp = 9.98		*Rwp* = 7.16
CM-10	*a* (Å)	5.3119(55)	5.2241(25)	5.4800(69)	*
	b (Å)	9.2968(87)	9.0378(40)	8.933(11)	
	c (Å)	10.2163(44)	10.3077(58)	29.622(19)	
	β (°)	99.992(67)	99.209(58)	97.93(14)	
	Cell vol. (Å)^3	496.86(73)	480.39(42)	1436.3(27)	
			Rwp = 4.33		

Parameters are calculated using the *TOPAS* (2009) software. Standard deviations are given in parentheses.
Rwp: agreement weighted profile factor in the Rietveld method. *insufficient profile intensity for vermiculite.

https://doi.org/10.1180/claymin.2016.051.5.05 Published online by Cambridge University Press

TABLE 3. Representative EMPA analyses of the pure micas (annite and phlogopite) from Catanda.

	Annite		Phlogopite					
Sample	CAT-60M	CM-27	AC-33	AC-34	AC-55	CAT-60	CM-26	CM-27
Al_2O_3	14.680	13.690	10.830	10.670	14.390	9.480	12.390	12.130
SiO_2	35.960	36.490	41.810	41.990	36.640	42.620	41.290	41.690
CaO	0.339	0.927	0.694	0.626	0.000	0.288	0.283	0.000
TiO_2	1.870	1.463	0.481	0.521	4.080	0.367	1.031	1.285
Na_2O	0.088	0.022	0.058	0.175	0.234	0.336	0.044	0.101
MgO	10.070	9.250	19.530	20.350	13.630	18.410	17.740	25.090
F	0.641	0.142	2.630	3.260	0.967	5.510	2.360	1.960
MnO	0.670	0.366	1.012	0.696	0.158	0.404	0.936	0.271
FeO*	20.900	20.490	8.710	8.920	16.620	12.450	12.370	5.130
BaO	0.130	0.087	0.021	0.000	0.179	0.132	0.031	0.015
K_2O	7.610	7.060	7.630	8.190	8.430	8.690	8.550	7.980
SrO	0.051	0.086	0.080	0.037	0.000	0.088	0.087	0.042
Cr_2O_3	0.019	0.016	0.019	0.027	0.009	0.008	0.000	0.034
Total	93.028	90.088	93.505	95.462	95.338	98.784	97.111	95.727
Number of cations on the basis of 12 (O, OH, F)								
Si	2.843	2.946	3.140	3.118	2.782	3.188	3.038	2.979
^{IV}Al	1.157	1.054	0.860	0.882	1.218	0.812	0.962	1.021
^{VI}Al	0.210	0.249	0.098	0.052	0.069	0.024	0.113	0.001
Ti	0.111	0.089	0.027	0.029	0.233	0.021	0.057	0.069
$^{VI}Fe^{2+}$	1.382	1.384	0.547	0.554	1.055	0.779	0.761	0.307
Mn	0.045	0.025	0.064	0.044	0.010	0.026	0.058	0.016
^{VI}Mg	1.187	1.113	2.186	2.253	1.543	2.053	1.946	2.605
Cr	0.001	0.001	0.001	0.002	0.001	0.000	0.000	0.002
$\sum VI$	2.936	2.861	2.924	2.933	2.911	2.903	2.936	3.000
$^{VI}Mg/(Mg+Fe^{2+})$	0.462	0.446	0.800	0.803	0.594	0.725	0.719	0.895
^{Int}Mg	0.000	0.000	0.000	0.000	0.000	0.000	0.000	0.067
Ba	0.004	0.003	0.001	0.000	0.005	0.004	0.001	0.000
Ca	0.029	0.080	0.056	0.050	0.000	0.023	0.022	0.000
Na	0.013	0.003	0.008	0.025	0.034	0.049	0.006	0.014
K	0.767	0.727	0.731	0.776	0.816	0.829	0.803	0.727

(continued)

TABLE 3. (*contd.*)

	Annite		Phlogopite					
Sample	CAT-60M	CM-27	AC-33	AC-34	AC-55	CAT-60	CM-26	CM-27
Sr	0.002	0.004	0.003	0.002	0.000	0.004	0.004	0.002
∑interlayer cation	0.816	0.818	0.799	0.852	0.856	0.909	0.836	0.811
interlayer charge	0.851	0.905	0.859	0.904	0.862	0.940	0.863	0.880
F	0.160	0.036	0.625	0.766	0.232	1.304	0.549	0.443
OH	1.840	1.964	1.375	1.234	1.768	0.696	1.451	1.557

FeO* = total iron.

phlogopite does not form interstratified structures but generates a mixture of phlogopite and vermiculite end-members consisting of intergrowths of both minerals in an intermediate stage of alteration, similar to the intergrowth of phyllosilicates described by Giorgetti *et al*. (1997) and Hillier *et al*. (2013).

Vermiculite generated by the alteration of phlogopite is enriched in Ca, while Mg and Na are present in minor amounts. It has d_{002} values of 14.6–14.8 Å, which are intermediate compared to reported d_{002} values of Ca-vermiculite (15.07 Å) and Mg-vermiculite (14.33 Å) (Deer *et al*., 1962; MacEwan and Wilson, 1980). This difference is attributed to the entry of Ca and Mg in the interlayer space of vermiculite (Tables 4 and 5). Ca enrichment in the Catanda vermiculite was probably produced by the abundance of calcite, which is the main mineral phase in the carbonatitic pyroclastic rocks (68–87 wt.%).

The release of interlayer K^+ and its corresponding replacement by other cations would be generated by diffusion (Douglas, 1989), which may have been produced in two different ways. In the first possible case, K^+ was diffused from all the interlayer spaces and the mica evolved directly to vermiculite. In the second case, K^+ could have diffused along specific (001) planes – not along the adjacent (001) planes – generating an interstratified grain of mica-vermiculite (Azzone & Ruberti, 2010). Whereas the intermediate products of phlogopite vermiculitization reported by Moon *et al*. (1994) and Azzone & Ruberti (2010) fit with the second case, the view of the present authors is that the alteration of Catanda phlogopite followed the first process, in particular because no interstratified phlogopite-vermiculite was identified.

Vermiculitization of annite

The alteration of annite leads to the formation of grains of annite/K-vermiculite that are generally expanded, presenting typical accordion textures (Fig. 3c2). The composition is clearly different from Ca-vermiculite, with #Mg < 0.5 and K_2O contents of > 5 wt.%. The annite/K-vermiculite grains are considered to be intermediate products between annite and K-vermiculite, and can also be identified using XRD by a d_{002} spacing of 10 Å. The d_{002} spacing of vermiculite is directly dependent on interlayer cation: 14.33 Å for Mg-vermiculite, 15.07 Å for Ca-vermiculite, 12.56 Å for Ba-vermiculite, 12.56 Å for Na-vermiculite, and 10.42 Å for K-vermiculite (Barshad, 1948; Deer *et al*., 1962). Ca-vermiculite and Mg-vermiculite contain two layers of water molecules, Ba-,

https://doi.org/10.1180/claymin.2016.051.5.05 Published online by Cambridge University Press

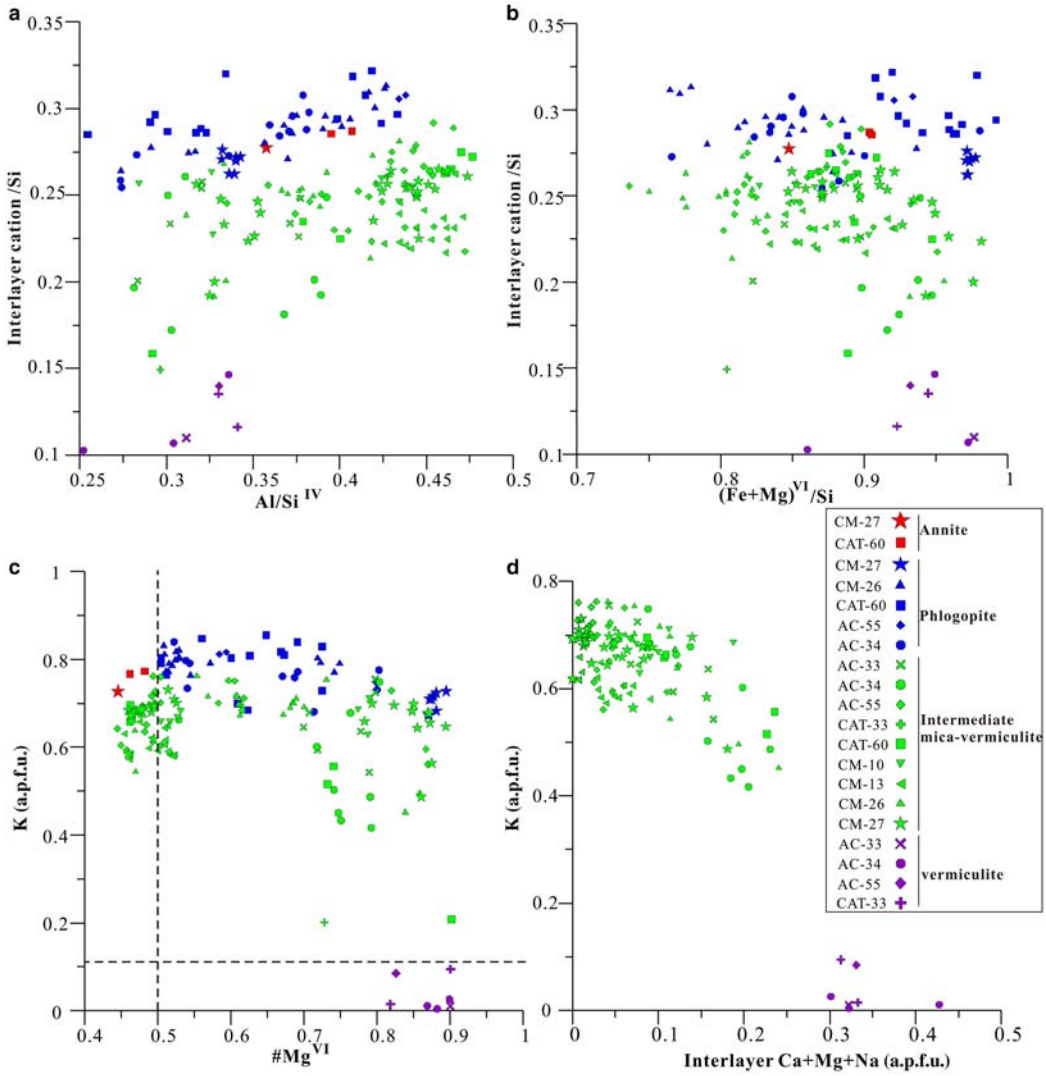

FIG. 7. Compositional diagrams of: (a) Al/Si *vs*. interlayer cation/Si; (b) $(Fe + Mg)^{VI}$/Si *vs*. interlayer cation/Si; (c) $\#Mg^{VI}$ *vs*. K (a.p.f.u.); the vertical line at #Mg = 0.5 defines the annite and phlogopite fields, while the horizontal line shows the limit of pure vermiculite at K = 0.125 a.p.f.u.; (d) Mg + Ca + Na *vs*. K (a.p.f.u.) in the interlayer position of vermiculite and intermediate mica-vermiculite.

Na- and Li-vermiculite present only one layer and $(NH4)^{+}$-, K-, Rb- and Cs-vermiculite do not contain interlayer water (Barshad, 1948; Deer *et al*., 1962). Marcos *et al*. (2009) divided commercial vermiculite in two different types: type-1 with K < 1 and Mg as the main interlayer cation and type-2 with K ≥ 1 and variable contents of interlayer Na, Ca or Mg. Marcos *et al*. (2009) also studied a vermiculite sample called China E, with 6.4 wt.% K_2O and a d_{002} spacing of 10.2 Å, which has similar features to the altered annite studied in Catanda. China E vermiculite has been identified as a type-2 vermiculite and it was also interpreted as a dehydrated vermiculite with no water or just a single layer of water molecules (Marcos *et al*., 2009). In the present study the d_{002} spacing of 10.07 Å corresponds to annite and phlogopite, but it could also

https://doi.org/10.1180/claymin.2016.051.5.05 Published online by Cambridge University Press

TABLE 4. Representative EMPA analyses of the Catanda vermiculite.

	AC-33C	AC-34I	AC-34H	AC-55M	CAT-33
Al_2O_3	10.320	11.580	9.420	10.420	12.370
SiO_2	39.050	38.840	39.360	37.170	39.930
CaO	2.750	2.660	3.420	3.740	3.720
TiO_2	0.304	0.521	0.196	0.539	0.490
Na2O	0.228	1.390	0.158	0.056	0.240
MgO	23.520	21.480	20.040	19.190	20.230
F	0.998	0.899	1.220	1.450	–
MnO	0.161	0.213	0.157	0.589	0.230
FeO*	4.710	5.790	4.770	7.570	8.000
BaO	0.000	0.014	0.063	0.022	–
K_2O	0.103	0.108	0.038	0.825	0.150
SrO	0.042	0.000	0.000	0.049	–
Cr_2O_3	0.010	0.010	0.000	0.007	0.070
Total	82.196	83.505	78.841	81.626	85.430
Number of cations on the basis of 12 (O, OH, F)					
Si	3.043	2.994	3.195	2.989	2.983
^{IV}Al	0.948	1.006	0.805	0.987	1.017
$^{IV}Fe^{3+}$	0.010	0.000	0.000	0.024	0.000
^{VI}Al	0.000	0.046	0.096	0.000	0.072
Ti	0.018	0.030	0.012	0.033	0.028
$^{VI}Fe^{3+}$	0.297	0.373	0.324	0.485	0.500
Mn	0.011	0.014	0.011	0.040	0.015
^{VI}Mg	2.674	2.469	2.425	2.300	2.253
Cr	0.001	0.001	0.000	0.000	0.004
$\sum$ VI	3.000	2.933	2.867	2.858	2.871
$^{VI}Mg/(Mg + Fe^{3+})$	0.900	0.869	0.882	0.826	0.818
^{Int}Mg	0.058	0.000	0.000	0.000	0.000
Ba	0.000	0.000	0.002	0.001	–
Ca	0.230	0.220	0.297	0.322	0.298
Na	0.034	0.208	0.025	0.009	0.035
K	0.010	0.011	0.004	0.085	0.014
Sr	0.002	0.000	0.000	0.002	–
$\sum$ interlayer cation	0.334	0.438	0.328	0.418	0.347
interlayer charge	0.624	0.659	0.628	0.744	0.645
F	0.246	0.219	0.313	0.369	–
OH	1.754	1.781	1.687	1.631	2.000

FeO* = total iron.

be interpreted as interstratified annite and K-vermiculite, as an intergrowth of annite and K-vermiculite, or simply as K-vermiculite.

Expansion of mica-vermiculite (polyphase 'vermiculite')

Pure vermiculites have little ability to expand but do increase in polyphase intergrowths, which are defined as intra-particle mosaics between mica and vermiculite (Hillier *et al*., 2013).

Rapid heating (to >300°C) may generate the expansion of mica-vermiculite intergrowths but the the same affect can also be achieved by means of chemical agents (Deer *et al*., 1966; Hillier *et al*., 2013). Nevertheless, because Catanda vermiculite-mica intergrowths are included in pyroclastic carbonatites related to volcanic eruptions (Campeny *et al*., 2014, 2015), a

https://doi.org/10.1180/claymin.2016.051.5.05 Published online by Cambridge University Press

TABLE 5. Interlayer cation compositions of the phlogopite and vermiculite analyses represented in Fig. 4a,b.

Interlayer cation (a.p.f.u.)		K	Ca	Mg	Na	Ba	Sr
Fig. 4a (AC-55M)	light grey laminae	0.728	0.000	0.000	0.005	0.000	0.000
	dark grey laminae	0.085	0.322	0.000	0.009	0.001	0.002
Fig. 4b (CAT-60J)	light grey centre	0.729	0.068	0.011	0.024	0.008	0.000
	dark grey border	0.066	0.232	0.046	0.029	0.001	0.066

hypothetical genetic model was also created (Figs 8 and 9) with accordions related to thermal expansion. In this case, the structural water of vermiculite would be converted to vapour by rapid heating and the mica acts as a barrier, generating high-pressure points and the corresponding expansion of the grains (Hillier *et al*., 2013) (Fig. 8).

In the model proposed here (Fig. 9), the vermiculitization of Catanda micas occurred before the expansion, during an early, supergene, general alteration of carbonatitic rocks and Archaean granites, which contain primary phlogopite and annite, respectively. Later, during late eruptive processes, thermal expansion of vermiculite occurred as a consequence of temperature increase by interaction with the rising new batch of carbonatititc magma. Finally, vermiculite accordions were deposited as pyroclastic materials and the interstitial space was filled by calcite cement which replaced all of the original vermiculite accordions (Fig. 9).

CONCLUSIONS

To the authors' knowledge, the accordion textures related to the expansion of vermiculite in the Catanda pyroclastic rocks are the first example of expanded vermiculite occurring under natural conditions.

The alteration of phlogopite in the Catanda pyroclastic carbonatites generated intergrowths of phlogopite and Ca-vermiculite, but no interstratified structures (because of the lack of any XRD peaks at 12 Å). The progressive vermiculitization of the phlogopite led to the leaching of K and the corresponding increase in Ca contents, and the vermiculite-phlogopite intergrowths stimulated the

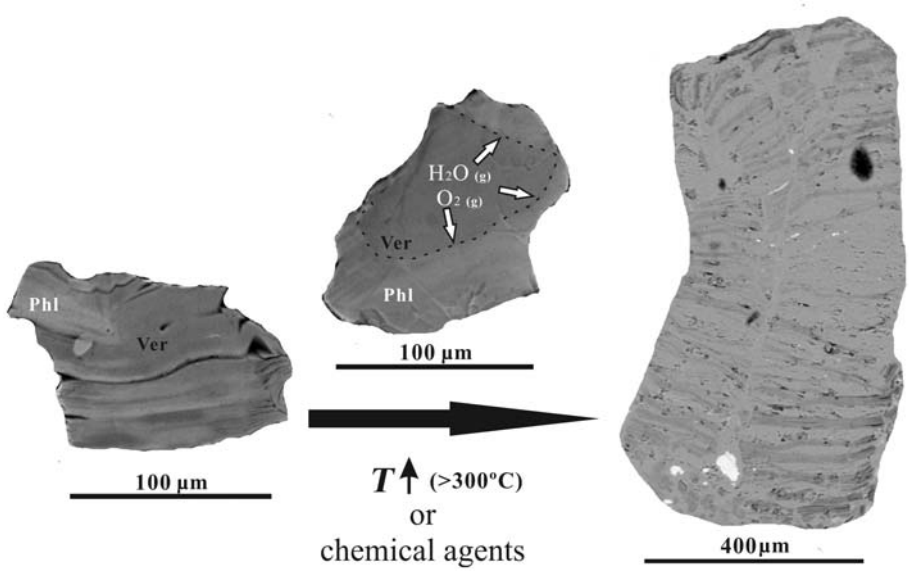

FIG. 8. Model proposed for the Catanda accordions (adapted from the process proposed by Hillier *et al*. (2013)), based on the expansion of polyphase vermiculite, which, in this case, is formed from an intergrowth of phlogopite (Phl) and vermiculite (Ver).

https://doi.org/10.1180/claymin.2016.051.5.05 Published online by Cambridge University Press

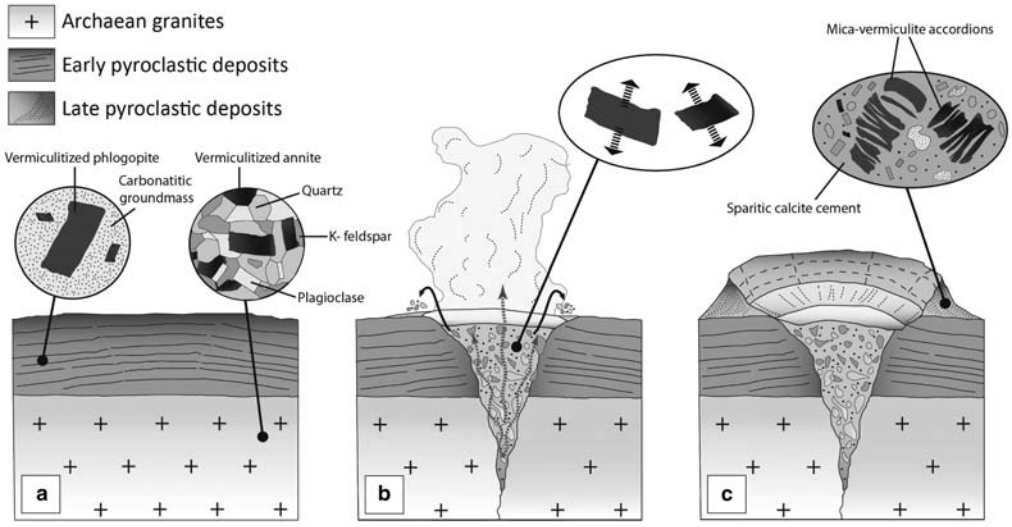

FIG. 9. Schematic diagram showing the generation of mica-vermiculite accordions during the Catanda carbonatitic volcanism. (a) Vermiculitized phlogopite and annite grains in carbonatitic rocks and Archaean granites, respectively. (b) Development of volcanic eruptive processes associated with carbonatitic magmatism. Thermal expansion of mica-vermiculite intergrowths. (c) Deposition of expanded mica-vermiculite intergrowths in the carbonatitic pyroclastic materials. The interstitial space is filled by sparitic carbonatitic calcite.

generation of the accordion textures produced by expansion. The annite altered to K-vermiculite; the intermediate product could be interstratified or intergrowth annite and K-vermiculite as they cannot be differentiated from the diffraction maximum at 10 Å.

The formation of these accordions is related directly to the volcanic processes that occurred in the Catanda area. It is suggested, therefore, that rapid heating caused the expansion of the vermiculite.

ACKNOWLEDGEMENTS

The authors thank Xavier Llobet of the Scientific and Technical Centres of the University of Barcelona (CCiTUB), Spain, for his assistance with the EMPA analyses. The present study was supported by the research group SGR-444 of the Generalitat de Catalunya (Spain). Assistance during the fieldwork was provided by the Departamento de Geologia da Universidade Agostinho Neto from Luanda, Angola. The authors are also very grateful to Fernando Nieto and an anonymous referee for their critical comments.

REFERENCES

Azzone R.G. & Ruberti E. (2010) Evolução Composicional dos Filossilicatos no Perfil Intempérico do Complexo Ultramáfico Alcalino-carbonatítico de Catalão I (GO). *Geologia USP, Série Científica*, **10**, 23–43.

Bailey S.W. (1980) Structures of layer silicates. Pp. 1–123 in: *Crystal Structures of Clay Minerals and their X-ray Identification* (G.W. Brindley & G. Brown, editors). Monograph **5**, Mineralogical Society, London.

Barshad I. (1948) Vermiculite and its relation to biotite as revealed by Base Exchange reactions, X-ray analyses, differential thermal curves and water content. *American Mineralogist*, **33**, 655.

Brigatti M.F., Frigieri P., Ghezzo C. & Poppi L. (2000) Crystal chemistry of Al-rich biotites coexisting with muscovites in peraluminous granites Sample: B1. *American Mineralogist*, **85**, 436–448.

Campeny M., Mangas J., Melgarejo J.C., Bambi A., Alfonso P., Gernon T. & Manuel J. (2014) The Catanda extrusive carbonatites (Kwanza Sul, Angola): an example of explosive carbonatitic volcanism. *Bulletin of Volcanology*, **76**, 818–834.

Campeny M., Kamenetsky V.S., Melgarejo J.C., Mangas J., Manuel J., Alfonso P., Kamenetsky M.B., Bambi A. & Gonçalves A.O. (2015) Carbonatitic lavas in Catanda (Kwanza Sul, Angola): Mineralogical and geochemical constraints on the parental melt. *Lithos*, **232**, 1–11.

Chakhmouradian A.R. (2006) High-field-strength elements in carbonatitic rocks: Geochemistry, crystal chemistry and significance for constraining the sources of carbonatites. *Chemical Geology*, **235**, 138–160.

https://doi.org/10.1180/claymin.2016.051.5.05 Published online by Cambridge University Press

Deer W.A., Howie R.A. & Zussman J. (1962) *Rock-Forming Minerals, Vol. 3, Sheet Silicates*. Longman, London, pp. 246–255.

Deer W.A., Howie R.A. & Zussman J. (1966) *An Introduction to the Rock-Forming Minerals*. Longman, London, pp. 270–273.

Douglas L.A. (1989) Vermiculites. Pp. 635–674 in: *Minerals in Soils Environments* (J.B. Dixon & S.B. Weed, editors). Soil Science Society of America, Madison, Wisconsin, USA.

Giorgetti G., Memmi I. & Nieto F. (1997) Microstructures of intergrown phyllosilicate grains from Verrucano metasediments (northern Apennines, Italy). *Contributions to Mineralogy and Petrology*, **128**, 127–138.

Guggenheim S., Adams J.M., Bain D.C., Bergaya F., Brigatti M.F., Drits V.A., Formoso M.L.L., Galán E., Kogure T. & Stanjek H. (2006) Summary of recommendations of nomenclature committees relevant to clay mineralogy: report of the Association Internationale pour l'etude des Argiles, nomenclature committee for 2006. *Clay Minerals*, **41**, 863–877.

Hillier S., Marwa E.M.M. & Rice M. (2013) On the mechanism of exfoliation of "vermiculite". *Clay Minerals*, **48**, 563–582.

Hindman J.R. (2006) Vermiculite. Pp. 1015–1026 in: *Industrial Minerals and Rocks: Commodities, Markets and Uses*, 7th edition (J. Elzea Kogel, N.C. Trivedi, M.J. Barker & S. Krukowski, editors). Society of Mining, Metallurgy and Exploration, Littleton, Colorado, USA.

Hülsemann J. (1966) On the routine analysis of carbonates in unconsolidated sediments. *Journal of Sedimentary Research*, **36**, 622–625.

Huo X., Wu L., Liao L., Xia Z. & Wang L. (2012) The effect of interlayer cations on the expansion of vermiculite. *Powder Technology*, **224**, 241–246.

MacEwan D.M.C. & Wilson M.J. (1980) Interlayer and intercalation complexes of clay minerals. Pp. 197–248 in: *Crystal Structures of Clay Minerals and their X-ray Identification*, (G.W. Brindley & G. Brown, editors). Monograph **5**, Mineralogical Society, London.

Marcos C. & Rodríguez I. (2010) Expansion behaviour of commercial vermiculites at 1000°C. *Applied Clay Science*, **48**, 492–498.

Marcos C., Arango Y.C. & Rodríguez I. (2009) X-ray diffraction studies of the thermal behaviour of commercial vermiculites. *Applied Clay Science*, **42**, 368–378.

Moon H.S., Song Y. & Lee S.Y. (1994) Supergene vermiculitization of phlogopite and biotite in ultramafic and mafic rocks, Central Korea. *Clays and Clay Minerals*, **42**, 259–268.

Nelson D.R., Chivas A.R., Chappell B.W. & McCulloch M.T. (1988) Geochemical and isotopic systematics in carbonatites and implications for the evolution of ocean-island sources. *Geochimica et Cosmochimica Acta*, **52**, 1–17.

Powder Diffraction File, version 2 (2000) Joint Committee of Powder Diffraction Standards. 12 Campus Blvd, Newtown Square, PA 19073, USA.

Rieder M., Cavazzini G., D'Yakonov Y.S., Frank-Kamenetskii V.A., Gottardi G., Guggenheim S., Koval P.V., Müller G., Neiva A.M.R., Radoslovich E.W., Robert J.-L., Sassi F.P., Takeda H., Weiss Z. & Wones D.R. (1998) Nomenclature of the micas. *The Canadian Mineralogist*, **36**, 905–912.

Rieder M., Cavazzini G., D'yakonov Yu.S., Frank-Kamenetskii V.A., Gottardi G., Guggenheim S., Koval P.V., Mueller G., Neiva A.M.R., Radoslovich E.W., Robert J.-L., Sassi F.P., Takeda H., Weiss Z. & Wones D.R. (1999) Nomenclature of the micas. *Mineralogical Magazine*, **63**, 267–279.

Schingaro E., Scordari F. & Ventruti G. (2001) Trioctahedral micas-1M from Mt. Vulture (Italy): Structural disorder and crystal chemistry Sample: LC2G Locality: Mt. Vulture, Italy. *European Journal of Mineralogy*, **13**, 1057–1069.

Shirozu H. & Bailey S.W. (1966) Crystal structure of a two-layer Mg-vermiculite. *American Mineralogist*, **51**, 1124–1143.

Silva M.V.S. & Pereira E. (1973) Estrutura Vulcânico-Carbonatitica da Catanda (Angola). *Boletim dos Serviços de Geologia e Minas de Angola*, **24**, 5–14.

Thorez J. (1975) *Phyllosilicates and Clay Minerals: A Laboratory Handbook for their X-ray Diffraction Analysis* (G. Lelotte, editor), pp. 23–34. B 4820 Dison, Belgium.

Tischendorf G., Förster H.-J., Gottesmann B. & Rieder M. (2007) True and brittle micas: composition and solid-solution series. *Mineralogical Magazine*, **71**, 285–320.

Toksoy-Köksal F., Türkmenoglu A.G. & Göncüoglu M.C. (2001) Vermiculitization of phlogopite in metagabbro, Central Turkey. *Clay Minerals*, **49**, 81–91.

TOPAS (2009) General Profile and Structure Analysis Software for Powder Diffraction Data, version 4.2, Bruker AXS Gmbh, Karlsruhe, Germany, 2009.

Walker G.F. (1951) Vermiculites and some related mixed-layer minerals. Pp. 199–223 in: *X-ray Identification and Crystal Structures of Clay Minerals* (G.W. Brindley, editor). Mineralogical Society, London.

Woolley A.R. & Church A.A. (2005) Extrusive carbonatites: a brief review. *Lithos*, **85**, 1–14.

Wyllie P.J., Jones A.P. & Dent J. (1996) Rare earth elements in carbonate-rich melts from mantle to crust. Pp. 77–102 in: *Rare Earth Minerals: Chemistry, Origin and ore Deposits* (A.P. Jones, F. Wall & C.T. Williams, editors). Chapman & Hall, London.

X'Pert HighScore Plus, version 2.2.2 (2006) PANalytical B.V. Almelo, The Netherlands.